Elsevier Editorial System(tm) for Journal of Hydrology
Manuscript Draft

Manuscript Number: HYDROL8114R1

Title: The hydrology of the proglacial zone of a High-Arctic glacier (Finsterwalderbreen, Svalbard): atmospheric and surface water fluxes.

Article Type: Research Paper

Keywords: Arctic; Svalbard; proglacial; precipitation; runoff; evaporation.

Corresponding Author: Dr. Richard Hodgkins,

Corresponding Author's Institution: Loughborough University

First Author: Richard Hodgkins

Order of Authors: Richard Hodgkins; Richard Cooper; Jemma Wadham; Martyn Tranter

# The hydrology of the proglacial zone of a High-Arctic glacier (Finsterwalderbreen, Svalbard): atmospheric and surface water fluxes.

Richard Hodgkins[a1]
Richard Cooper[b]
Jemma Wadham[c]
Martyn Tranter[c]

[a]Department of Geography, Loughborough University, Leicestershire, LE11 3TU, U.K.
[b]The Macaulay Institute, Craigiebuckler, Aberdeen, AB15 8QH, U.K.
[c]School of Geographical Sciences, University of Bristol, Bristol, BS8 1SS, U.K.

[1]Corresponding author: r.hodgkins@lboro.ac.uk, tel. +44-(0)1509-222753, fax +44-(0)1509-223930.

**Abstract**

Proglacial areas are expanding globally as a consequence of sustained glacier retreat, but there are very few studies focusing on their hydrology. This paper examines the surface and atmospheric water fluxes over a complete annual cycle in the proglacial area of the Svalbard glacier Finsterwalderbreen (77° N), through a combination of field measurements, physical modelling and statistical estimation. Precipitation in winter (226 mm) exceeded that in summer (29 mm), and over the course of the annual cycle total precipitation exceeded total evaporation (141 mm), although evaporative outputs from the proglacial area exceeded precipitation inputs during the dry summer. Runoff was highly irregular in time, with much of the total annual flow being concentrated into two relatively brief, early-to-mid summer intervals, the greater of which was characterised by the release of subglacially-stored water. Water fluxes were dominated by meltwater supply from the glacier: the total annual glacial runoff ($7.38 \times 10^7$ m$^3$) was an order-of-magnitude greater than the precipitation flux delivered directly to the proglacial area, and two orders-of-magnitude greater than evaporative losses from it. Outputs of meltwater from the proglacial area were not significantly different from inputs over the duration of the melt season, so surface water storage does not appear to be important in the studied catchment, despite episodes of flooding over shorter timescales. A synthesised description of the seasonal hydrological cycle in Finsterwalderbreen's proglacial area is presented, which can be viewed as a set of hydrological boundary conditions for comparable high-latitude locations. Further study of these conditions is required, because the challenging nature of hydrometry in the high-latitudes has the potential to limit progress in understanding environmental change there.

**Key words** Arctic, Svalbard, proglacial, precipitation, runoff, evaporation.

**PACS codes** 92.40.Vq, 92.40.We, 92.40.Zg

## 1. Introduction

### 1.1 Proglacial hydrology

Proglacial areas, located immediately in front of glaciers and strongly influenced by fluxes of water and sediment from them, are expanding globally as a consequence of sustained glacier retreat. Studies of specifically proglacial hydrology are few in number, reflecting the tendency for research in glacierized catchments to focus principally on glacial processes (e.g. Willis, 2005). Hydrological data from the Arctic are sparse even today, and in the Norwegian Arctic archipelago of Svalbard, for example, there are currently only 8 continuously-recording hydrometric stations, in 5 locations (Sund, 2008). Yet detailed information on the quantity of water stored as snow, ice, groundwater and in lakes, and on the exchange of water between these stores, from the atmosphere as precipitation and from catchments as evaporation and runoff, is important both for the development of Arctic communities and for scientific understanding of the Arctic hydrological cycle and its response to enhanced atmospheric warming (Anisimov et al., 2007; Bates et al., 2008).

Results from studies of glacial hydrology do provide information concerning the nature of meltwater inputs to the proglacial zone. Observations from Svalbard indicate that the annual thaw typically commences in early June (Repp, 1988; Vatne *et al.*, 1995; Hodgkins *et al.*, 1997), when air temperatures begin to rise consistently above zero (Hanssen-Bauer *et al.*, 1990). However, the onset of runoff typically lags the increase in energy inputs, since significant volumes of meltwater are temporarily stored in the snowpack and in various glacial reservoirs (Repp, 1988; Vatne *et al.*, 1996; Hodgkins, 2001; Hodson et al., 2005). Early season discharge may therefore be highly variable, with little indication of diurnal cycling until later in the melt season, when such stores are depleted. Results from numerous studies indicate that peak runoff typically occurs during July and August in Svalbard (Repp, 1988; Vatne *et al.*, 1995; Hodgkins *et al.*, 1997; Wadham *et al.*, 1997; Hodson et al., 1998; Hodgkins, 2001), when air temperatures are at a maximum (Hanssen-Bauer *et al.*, 1990). The sudden release of large volumes of stored meltwater to the proglacial zone from subglacial reservoirs has been observed during the summer (Wadham *et al.*, 2001).

The presence of cold, impermeable surface ice on many glaciers in Svalbard often results in a significant proportion of meltwater being directed to the margins and routed to the proglacial zone in lateral, ice-marginal channels (Hodgkins, 1997; Hagen et al., 2000). However, in instances where runoff is able to access the glacier bed, meltwater may be routed to the proglacial zone subglacially and may emerge under artesian pressure in front of the glacier terminus (Vatne *et al.*, 1995; Wadham *et al.*, 1998; Hodson et al., 2005). No direct observations of the annual freeze-up in Svalbard have been reported to date, although it is likely that the cessation of runoff occurs in early October, when air temperatures begin to fall consistently below zero (Hanssen-Bauer *et al.*, 1990). In some instances, stored meltwater may continue to issue from ice-marginal and subglacial reservoirs during the winter, forming extensive icings (*aufeis* or *naledi*) in the proglacial zone (Vatne *et al.*, 1995; Hodgkins *et al.*, 1997; Wadham *et al.*, 2000; Hodgkins et al., 2004; Hodson et al., 2005).

## 1.2 Aims

The purpose of this paper is to quantify and analyse the hydrology of the proglacial area of a high-arctic glacier, focusing on surface and atmospheric water fluxes. A combination of field measurements and modelling will be used to determine temporal variation in precipitation, evaporation and runoff over the course of an annual cycle, and daily and total cumulative fluxes of water from each of these sources will be quantified. This will lead to a synthesis of the annual proglacial surface hydrological regime. The subject of this study is the proglacial area of the Svalbard glacier Finsterwalderbeen: this glacier has already been the subject of a variety of glaciological and hydrological research over the past decade, including studies of its thermal regime (Ødegård *et al.*, 1997), surface and sub-surface hydrochemistry (Wadham et al., 1998, 2000, 2001; Cooper et al., 2002), fluvial sediment transfer (Hodson and Ferguson, 1999; Hodgkins et al., 2003), the spatial and temporal variation of winter accumulation (Hodgkins et al., 2005) and glacier dynamics (Nuttall et al., 1997; Nuttall and Hodgkins, 2005; Hodgkins et al., 2007). A companion paper will focus on sub-surface water fluxes in the proglacial area, and on the complete annual water budget.

## 2. Study site description

The proglacial zone of Finsterwalderbreen is located at 77º 31′ N, 15º 19′ E in Svalbard, Norway (Figure 1), and is part of a 65.7 km$^2$ (43.5 km$^2$ glacierized) catchment. The catchment is mostly devoid of vegetation, except above the most recent glacial trimline and on terminal moraines delimiting the proglacial zone, where a sparse Arctic flora survives. The bedrock geology is diverse, comprising Precambrian basement and Carboniferous through Cretaceous sedimentary units (Dallmann *et al*., 1990). The mean annual air temperature at 35 m a.s.l. is –3.9 °C, and mean monthly air temperatures are only positive during the summer, although even then they remain <6.0 °C (Hanssen-Bauer *et al*., 1990). Annual precipitation totals lie in the range 180-440 mm w.e., with the bulk being delivered as snow during the winter months (Hansen-Bauer *et al.*, 1990).

The proglacial zone itself consists of a sandur and a moraine complex situated between the glacier terminus and the coastline of Van Keulenfjorden (Figure 1); it has a total area of 4.3 km$^2$, most of which has only relatively recently been exposed by the retreat of the glacier from the limits of a surge event which occurred between 1898 and 1918 (Nuttall *et al*., 1997). The sediments comprising the proglacial zone contain material from all elements of the catchment lithology. The proglacial zone is underlain by permafrost, the upper layers of which thaw during the summer months to form a shallow active layer. The proglacial zone is constrained to the east, north and west by a series of compounded terminal moraines, which mark the limits of previous glacial advances. The remainder of the moraine complex comprises kames and kettles interspersed with relict outwash terraces and hummocky moraines. Many of the kettles and other depressions in this zone contain perennial lakes and pools, the largest of which has a surface area of 0.03 km$^2$. Many of these lakes and pools are connected by a network of small channels that convey surface runoff, which comprises varying proportions of snowmelt, rainfall and meltwater derived from in-situ thawing of the active layer, along a topographic gradient from the moraine complex to the sandur.

The sandur, which extends north-eastwards from the glacier terminus, is 1.5 km long and has a total area of 0.9 km$^2$, with an altitudinal range of 10–50 m a.s.l. The morphology of the sandur changes with increasing distance downstream, forming three distinct zones similar to those described by Krigstrom (1962) for Icelandic sandar. In the proximal zone, which extends approximately 0.5 km north-eastwards from the glacier terminus, runoff is conveyed mainly in a network of deep, narrow channels incised into coarse, gravelly sediments. In the intermediate zone, which extends approximately 0.5 km north-eastwards from the proximal zone, flow is conveyed in a network of braided channels incised into fine, sandy sediments. Many of these channels shift position frequently and some only convey flow during periods of high discharge. In the distal zone, which extends approximately 0.5 km north-eastwards from the intermediate zone, flow is conveyed in a network of very wide and ill-defined channels incised into fine, silty sediments. Many of these channels overflow during periods of high discharge, producing extensive areas of shallow flooding on the sandur surface. The channels in the distal zone converge where the sandur abuts the moraine complex to form a single well-defined channel, hereafter referred to as the Outlet (Figure 1), which breaches the terminal moraines before issuing into Van Keulenfjorden 1.5 km further downstream.

## 3. Methods

Meteorological time series were acquired over an 11-month period that included the 1999 melt season, in order to facilitate the calculation of total atmospheric water fluxes to and from the proglacial zone. Data concerning over-winter snow accumulation were acquired prior to the onset of the thaw associated with the 2000 melt season, in order to validate the use of regression relationships between altitude and snow depth derived from end-of-winter snow surveying conducted on the glacier in 1999, and thus facilitate the estimation of the total snowmelt water flux to the proglacial zone at the start of the 1999 melt season. Time series of discharge at points of input to and output from the proglacial channel network were acquired in order to facilitate the calculation of total surface water fluxes. Points of input comprised both the eastern and western ice-marginal channels at the glacier terminus (hereafter Terminus East and Terminus West), while all outputs were accounted for in the Outlet, where it breaches the terminal moraines (Figure 1).

### 3.1 Meteorological monitoring

An Automatic Weather Station (AWS) was sited in the moraine complex, approximately 0.75 km north of the glacier terminus (Figure 1), and operated for a total of 338 days, from 13:00 on day 113 (23 April) in 1999 to 20:00 on day 85 (25 March) in 2000. Air temperature and vapour pressure deficit were measured at a height of 2.0 m above the ground surface with a Campbell Scientific HMP45C temperature and relative humidity probe, housed within a Campbell Scientific URS1 unaspirated radiation shield. The potential error range for these measurements is ±2.0%, as specified by the instrument manufacturer. Global radiation (direct and diffuse), was also measured at a height of 2.0 m with a Kipp & Zonen SP-LITE pyranometer (potential error range ±2.5%). Wind speed was measured at a height of 2.2 m with an RM Young 05103 Wind Monitor (potential error range ±10.0%). Rainfall was measured from 17:00 on day 175 (24 June) to 12:00 on day 229 (17 August) during the 1999 melt season, using a Campbell Scientific ARG100 tipping bucket rain gauge (sensitivity 0.2 mm of water per tip). All variables were initially measured at 20-second intervals and compiled as hourly and daily means, with the exception of global radiation and rainfall, which were compiled as hourly and daily totals. From 16:00 on day 229 (17 August), the measuring interval was increased to 5 minutes and the compilation interval to four hours, in order to minimise power consumption and data storage in advance of the winter months.

### 3.2 Evaporation modelling

Actual evaporation is usually estimated as a fixed percentage of potential evaporation, or as a function of potential evaporation and soil moisture conditions. It may also be estimated as a residual term in a water balance calculation. However, evaporation measurements from Svalbard are "almost non-existent" (Killingtveit et al., 2003). For this study, daily evaporation fluxes from the surface of the proglacial zone were determined by summing hourly evaporation fluxes calculated using a modified version of the general combination model developed by Granger and Gray (1989) for non-saturated surfaces. To account for the departure from saturated conditions, this model makes use of the concept of relative evaporation (the ratio of actual evaporation to potential evaporation, the latter being defined as that which would occur under saturated conditions) and its relation to the relative drying power of the air (the ratio of the drying power of the air to the sum of the drying power of the air and total available energy from net radiation):

$$E = (\Delta E_r G_n / \Delta E_r + \gamma) + (\gamma E_r E_a / \Delta E_r + \gamma) \quad (1)$$

where $E$ is actual evaporation (mm h$^{-1}$), $\Delta$ is the slope of the saturation vapour pressure curve (mb °C$^{-1}$) (which defines the relationship between saturation vapour pressure and air temperature), $\gamma$ is the psychrometric constant (mb °C$^{-1}$), $E_a$ is the drying power of the air (mm h$^{-1}$), $G_n$ is the total available energy from net radiation (mm h$^{-1}$) and $E_r$ is relative evaporation. Full details of the method can be found in Granger and Gray (1989).

### 3.3 Unmonitored atmospheric water fluxes

Data concerning over-winter snow accumulation in the proglacial zone were not acquired prior to the onset of the thaw associated with the 1999 melt season. However, because the bulk of annual precipitation in this location is delivered as snow during the winter months, it is important that this component of the total atmospheric flux is estimated. Use was therefore made of snow depth and density data collected in end-of-winter surveys conducted on the glacier in 1999, and on the glacier and in the proglacial zone itself in 2000. Full details of how these data were collected are given in Hodgkins et al. (2005).

A frequently-encountered problem is that, while precipitation usually increases with elevation, most precipitation gauges are located in the lowlands (Killingtveit et al., 2003). Hanssen-Bauer et al. (1996) found that the ratio between true and measured precipitation at various sites in Svalbard varied between 1.26 for the summer and 1.70 for the winter. However, the proglacial zone considered here is a small area with a restricted elevation range (about 10–50 m a.s.l.): in summer, the precipitation gauge was located within the zone (Figure 1), while in winter, precipitation was measured directly by probing across the zone. Therefore the problematic extrapolation of precipitation data from a distant gauge is not necessary here.

Relationships between elevation and winter accumulation were assessed using linear regression models, using input data from 106 and 75 glacier-wide locations surveyed at the end of winter in 1999 and 2000 respectively, and used to estimate mean accumulation in the proglacial zone. The relationship is rather stable (1999 slope = 0.002, 2000 slope = 0.003; Table 1, Hodgkins et al., 2005), yielding similar accumulation estimates of 0.23 m w.e. (1999) and 0.24 m w.e. (2000). The mean end-of-winter snow depth in the proglacial zone in 2000, based on 39 probed locations over the interval from days 103–107 (12–16 April), was 0.25 m w.e., which is very close to the estimated depth and gives confidence that the regression model is valid over the limited elevation range of the proglacial zone. The potential error range for the snow depth measurements is estimated to be ±10.7%, as determined by averaging the standard errors from multiple measurements at all 39 locations.

The 1999 winter accumulation regression estimate is therefore regarded as reliable.

### 3.4 Discharge monitoring

Channel discharge was monitored in stable reaches for a total of 55 days, from 17:00 on day 175 (24 June) to 12:00 on day 229 (17 August). Stage was measured at each gauge at 20-second intervals using a Druck PDCR1830 pressure transducer (potential error ±0.1%) and compiled as hourly means. The stage records were converted into discharge time series using a rating curve (Table 1) derived from discrete velocity-area measurements using a Valeport BFM001 flow meter (potential error for velocity measurements is ±2.2%; the potential error range for the distance and depth measurements is estimated to be ±10%, due mainly to turbulent flow conditions).

At the Terminus gauges, damage inflicted to the instrumentation by rafted ice blocks and bedload, and recurrent channel migration, meant that stage records were only partly rated. Although intervals of missing data are typical in discharge time series from unstable, glacially-fed systems, a continuous record is required here to facilitate flux calculations. Short intervals of missing data (<12 hours) were interpolated geometrically (Synergy Software, 1997). Longer intervals of missing data at the Terminus East gauge were predicted from the continuous Outlet discharge record, using a linear regression model constructed using hourly input terms for the period from days 187–193 (6–12 July), as this excluded non-linear behaviour caused by stored water release (Wadham et al., 2001): Table 1. Longer intervals of missing data at the Terminus West gauge (>12 hours) were predicted from mass conservation (Table 1): this approach assumes that the sandur runoff budget is in steady-state and that inputs from water sources other than the ice-marginal channels are negligible. While results presented below indicate that the latter assumption is valid, observations of widespread flooding on the sandur during periods of high flow indicate that the former assumption is likely be invalid over shorter timescales (Cooper, 2003; Cooper et al., 2002).

### 3.5 Unmonitored surface water fluxes

Monitoring of channel discharge and glacial ablation commenced some time after the onset of the thaw associated with the 1999 melt season and ceased some time before the annual freeze-up. While surface water fluxes during these missed periods are likely to have been relatively small, the aims of assessing the full annual hydrological cycle and of fully quantifying all fluxes require that they be estimated.

Ablation on the glacier terminus was monitored for a total of 51 days, from days 178–228 (27 June–16 August), by measuring surface lowering at an aluminium stake every 2–4 days. The potential error range for ablation measurements is estimated to be ±10%, due mainly to uncertainty caused by surface roughness. Nevertheless, there are not enough data to model melt throughout the year at the scale of the entire glacier, so the approach taken was to find a relationship between melt on the terminus and runoff at the Outlet. A temperature-index model of melt on the glacier terminus was therefore developed, in order to estimate melt outside the monitoring period. Temperature-index melt models, which are based on empirical relationships between air temperature and ablation, have been widely applied in glacial environments and have proven to be powerful tools, despite their relative simplicity (Hock, 2003). In this instance, we used the model form

$$Abl = \begin{cases} f\left(T_a - T_0\right), & T_a > T_0 \\ 0, & T_a \leq T_0 \end{cases} \tag{2}$$

where *Abl* is specific melt (mm w.e.), *f* is a derived melt factor (the mean of individual ablation measurements divided by mean air temperature since the last measurement, mm w.e. °C$^{-1}$), $T_a$ is mean air temperature (°C) and $T_0$ is a threshold temperature beyond which melt is assumed to occur (in this case, 0 °C). An advantage of using this model form was the ease with which it enabled irregular time intervals in the measured ablation data to be simulated. The mean derived melt factor, 6.8 mm w.e. ˚C d$^{-1}$ (range 2.5–11 mm w.e. ˚C d$^{-1}$) is consistent with other reported degree-day factors for ice, which are in the range 5.4–20 mm w.e. ˚C $d^{-1}$ (Hock, 2003). The total modelled melt for the period of monitoring, 1722 mm, compares with the observed value of 1684 mm: a 3% difference. Linear regression of modelled melt on observed melt yields a highly significant ($p$<0.001) relationship with an $R^2$ value of 0.66. Model error, based on the Root-Mean-Squared Error (RMSE) expressed as a percentage of the mean observed melt, is ±21.5%. The performance of the melt model is therefore satisfactory, and daily values of ablation for the entire 1999 melt season were modelled using mean daily air temperature as the input series.

Daily discharge fluxes at the Outlet were then estimated from daily values of modelled ablation, using a regression relationship for the whole of the period during which ablation was monitored. The delay between ablation on the glacier terminus and flow response in the Outlet was accounted for by lagging the discharge series by 1 day. Linear regression of Outlet discharge on modelled melt yields a highly significant ($p$<0.001) relationship with an $R^2$ value of 0.74. The total modelled Outlet flux for the period of monitoring, $4.94\times10^7$ $m^3$, compares with the observed value of $4.79\times10^7$ $m^3$: a 3% difference. Model error (RMSE as a percentage of mean observed melt) is ±36.2%. The performance of the discharge regression model is therefore satisfactory, and it has been used to estimate unmonitored surface water fluxes.

## 4. Results: atmospheric and surface water fluxes

### 4.1 Temporal variation in meteorology

Time series of mean daily air temperature, vapour pressure deficit, wind speed and total daily global radiation and rainfall are presented in Figure 2. Mean daily air temperatures were consecutively positive (mean 4.7° C, range 0.5–10.4° C) during the period from days 156–262 (5 June–19 September), giving a duration for the 1999 melt season of 107 days. Outside this period, mean daily air temperatures were significantly lower (mean –5.7° C) and more variable (range –23.0 to 3.8° C). Mean daily vapour pressure deficits and mean daily wind speeds were high and variable during the melt season, especially on days when global radiation totals and mean air temperatures were high. Outside this period, both mean daily vapour pressure deficits and mean daily wind speeds were lower and less variable, reflecting more stable atmospheric conditions resulting from reduced daily global radiation totals and lower mean daily air temperatures. Daily global radiation totals were high and relatively invariable at the start of the period of monitoring, reflecting frequent clear-sky conditions and the receipt of significant quantities of diffuse radiation reflected by the snowpack. Daily global radiation totals gradually declined to zero with the onset of the polar night on day 296 (23 October). Rainfall was recorded on 15 days during the period from days 176–228 (25 June–16 August), although significant amounts only fell on three of these, with a maximum daily total of 8.0 mm (on day 226, 14 August).

Killingtveit et al. (2003) state that in Arctic catchments the summer potential evaporation may be very significant, due to high net radiation during days with 24 hours' sunlight, although actual evaporation may still be small as there is little vegetation, little rainfall and soils tend to dry up easily after snowmelt. Time series of total daily available energy and evaporation from the surface of the proglacial zone are presented in Figure 3. Daily evaporation totals were low at the start of the period of monitoring, reflecting the high albedo of the snowpack and the limited available energy. Following snowpack recession, daily evaporation totals became higher and more variable and remained so for the duration of the melt season. The maximum daily evaporation total was 4.4 mm on day 190 (9 July). Variability was largely driven by global radiation during this time interval, although rainfall and low mean daily vapour pressure deficits associated with the passage of maritime air masses from the south-west were intermittently significant. The mean daily total evaporation in the period from the start of June to the end of August was 1.4 mm. In the period between the end of the melt season and the onset of the polar night, daily evaporation totals declined rapidly to zero ahead of the gradual decline in daily global radiation totals, reflecting increasing long-wave radiative losses and the progressive cooling of the land surface during the annual freeze-up. Evaporation effectively stopped (daily totals ≤0.1 mm) on day 249 (6 September).

**4.2 Daily and cumulative atmospheric water fluxes**

Daily total rainfall and evaporation are presented in Figures 2(E) and 3(B), respectively. Since rainfall was only monitored in the 53-day period from day 176–228 (25 June–16 August), it is possible that a significant proportion of total annual rainfall was missed. Since there is no way of realistically predicting missed rainfall totals, the cumulative total recorded is considered to be a minimum estimate of total rainfall in 1999: the cumulative total of 29.4 mm equates to a total cumulative atmospheric water flux of $1.26 \times 10^5$ $m^3$ (assuming spatial representativeness). The highest daily rainfall flux ($3.44 \times 10^4$ $m^3$ on day 226 (14 August]) accounted for about 27% of the total cumulative atmospheric water flux.

Daily evaporation totals were determined for the entire period of monitoring, which included almost all of the period in which evaporation could occur. The total determined during the period of monitoring (141 mm) is therefore considered to equate to total annual evaporation in 1999, which in turn equates to a total cumulative atmospheric water flux from the proglacial zone of $6.08 \times 10^5$ $m^3$ (assuming spatial representativeness). The highest daily evaporation total (4.4 mm on day 190 [9 July]) corresponds to a total daily atmospheric water flux of $1.89 \times 10^4$ $m^3$ (about 3% of the total flux). During the 53-day period in which rainfall was monitored, a cumulative total of 98.7 mm of evaporation was recorded, which exceeds the cumulative rainfall total by about 240%. The estimated water-equivalent snow accumulation at the end of the 1999 winter season (226 mm) equates to a total atmospheric water flux to the proglacial zone of $9.70 \times 10^5$ $m^3$. Total annual precipitation (255 mm) therefore exceeded total annual evaporation (141 mm) by about 81% in 1999.

Various sources of potential error have been identified concerning the determination of atmospheric water fluxes to and from the proglacial zone, including those associated with the use of instrumentation, field techniques and empirical equations. With regard to the rainfall water flux, the main sources of potential error relate to the catch efficiency of the rain gauge and the fact that rainfall was only monitored for about 50% of the melt season: in the former case, it is reasonable to assume that the catch efficiency of the rain gauge was >95%, given that the mean wind speed on days when rain fell during the period of monitoring was low (2.71 m $s^{-1}$) (Bruce & Clark, 1990); in the latter case, it is conceivable that the annual rainfall total may have been about 100% greater than the monitored total, but given that the bulk of total annual precipitation in Svalbard comprises snowfall (Hanssen-Bauer *et al*., 1990), even a doubling of the rainfall total in this instance only generates a potential error range of ±20.2% for total annual precipitation. Since these various sources of potential error are multidirectional and therefore non-additive, realistic estimates of error may be determined by combining all of the potential errors probabilistically as the root of the sum of the squares of individual error sources (Topping, 1972). This approach gives a probable error for the rainfall water flux in the period of monitoring of ±20.8%.

With regard to the snowpack water-equivalent flux, the main sources of potential error relate to the high standard error associated with the snow-depth measurements and the fact that the snow depth was estimated from a regression on elevation. However, repeated measurements in 1999 and 2000 showed that it was the spatial variation of accumulation which contributed by far the most to overall error, being greater, for instance, than inter-annual variability (Hodgkins et al., 2005). Killingtveit et al. (2003) make the same point in suggesting that residual errors in water balance calculations are probably related mainly to problems of precipitation correction. The probable error range for the snowpack flux may therefore be estimated by combining the standard errors associated with the snow depth and density measurements probabilistically, giving ±43.7% (the greatest proportional uncertainty of all the fluxes). With regard to the evaporation flux, the main potential sources of error relate to the use of instrumentation and empirical equations, the latter of which include potential errors associated with assumed values and approximations, in addition to an overall standard error. Probable errors for the evaporation flux are summarised in Table 2.

### 4.3 Temporal variation in runoff

Time series of discharge at points of input to and output from the proglacial channel network are presented in Figure 4. The seasonal pattern of discharge was characterised by two periods of high and variable flow interspersed with periods of low and relatively invariable flow. The first period of high flow occurred during the first 11 days of monitoring, over days 175–186 (24 June–5 July). During the first 4 days of this period, peak daily discharge at the Outlet rose rapidly from <5 $m^3 s^{-1}$ to >33 $m^3 s^{-1}$ and diurnal cycling became evident. Weather conditions during this period were warm and windy (Figure 2) and the snowline was observed to retreat rapidly up the lower reaches of the glacier. Localised flooding was observed on the sandur in the time interval from days 179–180 (28–29 June). The second period of high flow occurred during the middle of the melt season, over days 195–207 (14–26 July). During the first 4 days of this period, weather conditions were again warm and windy and peak daily discharge at the Outlet rose dramatically from <11 $m^3 s^{-1}$ to its seasonal maximum of >60 $m^3 s^{-1}$ at 20:00 on day 199 (18 July): massive bank erosion was observed at the Terminus West gauge on this day, along with large numbers of rafted ice blocks and enhanced turbidity (Hodgkins et al., 2003). Wadham et al. (2001) have described the occurrence of seasonal outburst floods from Finsterwalderbreen, with the hydrochemical signature of released waters suggesting a subglacial origin. Widespread flooding was observed on the sandur during the time interval from days 199–202 (18–21 July). In contrast to these high-magnitude events, flow in the intervening periods was relatively low and invariable, save for increasingly well-defined diurnal cycling.

## 4.4 Daily and cumulative surface water fluxes

Total daily glacier ablation (measured and modelled) and total daily surface water flux from the proglacial zone (measured and estimated) are presented in Figure 5. A total cumulative water flux of $4.79 \times 10^7$ m$^3$ was discharged at the Outlet gauge during the 53-day period from days 176–228 (25 June–16 August). During the same time interval, a combined total cumulative water flux of $4.88 \times 10^7$ m$^3$ was discharged at the Terminus West and Terminus East gauges (about 64% at the West and 36% at the East). The difference between the total cumulative water fluxes at the Terminus and Outlet gauges of $0.09 \times 10^7$ m$^3$ (about 2% of the total cumulative flux at the Outlet) falls well within the probable error range for discharge determined at all three gauges (Table 3), so is not regarded as significant. During the 51-day period from days 178–228 (27 June–16 August), a cumulative total of 1.68 m w.e. ablation was recorded on the glacier terminus. Some 0.6 km$^2$ of the terminus was drained by supraglacial channels flowing directly to the proglacial channel network, i.e. water which was not accounted for at the Terminus West or East gauges. This gives a total cumulative supraglacial water flux of $1.01 \times 10^6$ m$^3$: only 2% of the combined flux at the Terminus gauges during the same time interval. During the first period of high flow, a total water flux of $1.15 \times 10^7$ m$^3$ (about 24% of the total cumulative flux) was discharged at the Outlet. During the second period of high flow, a total water flux of $2.16 \times 10^7$ m$^3$ (about 45% of the total cumulative flux in less than 23% of the monitoring period) was discharged at the Outlet. Of this total, $3.91 \times 10^6$ m$^3$ (about 8% of the total cumulative flux) was discharged in one day (day 199, 18 July, <2% of the monitoring period), when discharge at the Outlet attained its seasonal maximum.

A total estimated water flux of $2.42 \times 10^7$ m$^3$ was discharged at the Outlet outside the period of monitoring (Figure 5). Summing the combined unmonitored water fluxes and the cumulative water flux at the Outlet during the period of monitoring gives a total annual flux of $7.21\times10^7$ $m^3$. Of this total, about 9% was discharged prior to the onset of monitoring, about 66% was discharged during the period of monitoring and about 25% was discharged after its cessation. It is likely that predicted peaks and troughs in runoff outside the period of monitoring are over- and under-estimates respectively, as they cannot take into account the variable, modulating effect of meltwater storage, and therefore that flow in the missed periods was relatively low and invariable.

Numerous sources of potential error have been identified concerning the acquisition of time series of discharge in both melt seasons, including those associated with the use of instrumentation, field techniques and statistical procedures. Probable errors for the surface water flux are summarised in Table 3. There is unquantifiable error associated with the melt model (aside from the error determined by comparison with observed melt) from the use of a melt factor derived from ablation measurements from an ice surface: this likely over-predicts melt early in the summer when the glacier is still snow-covered. On the other hand, only 9% of total runoff is estimated to occur in the period prior to the commencement of monitoring, so there is unlikely to be a significant impact on the magnitude of the calculated flux. The melt factor should be appropriate for the period after the cessation of monitoring, when glacier ice is exposed.

## 5. Synthesis: the annual proglacial hydrological regime at Finsterwalderbreen

The data presented above provide insights into the nature of the annual proglacial hydrological regime at Finsterwalderbreen, particularly in terms of the significance of diverse hydrological pathways in both space and time. The following discussion synthesises these data with field observations and results from previous studies to produce a qualitative framework outlining the principal variations in surface hydrology in the proglacial zone of Finsterwalderbreen over the course of an annual cycle. This framework can be used as a context for understanding fluvial material fluxes from this and similar catchments, and as a basis for assessing the effects of climate change on local and regional hydrological regimes.

### 5.1 Winter (December–March)

Winter is essentially a dormant phase in the annual proglacial hydrological cycle. During the winter months, when mean air temperatures are at an annual minimum and continuous darkness prevails, the ground surface in the proglacial zone remains entirely frozen and blanketed by snow cover down to sea level. The only significant hydrological events are the development of an icing in the area where the western ice-marginal channel issues into the proglacial channel network, and the receipt of significant quantities of snowfall, typically in mid-to-late winter (February–March). The development of the icing occurs as a result of the freezing of subglacial drainage, which issues throughout the winter from an artesian upwelling situated at the glacier terminus (Wadham *et al*., 2000). Some additional water is supplied to the icing by snowmelt on the glacier terminus during warmer periods associated with the passage of maritime air masses (Wadham *et al*., 2000). Ice layers form beneath and within the proglacial snowpack during such periods, as snowmelt percolates downwards and then refreezes. Sublimation may occur, but to what extent is unknown: some estimates suggest that up to about 20 % of winter snowfall may be lost by sublimation in situations where air humidity is very low (French, 2007). The return of daylight in mid-February following the cessation of the polar night has little initial impact on hydrological activity in the proglacial zone, since the progressive increase in the receipt of energy inputs from solar radiation is very gradual and largely offset by the high albedo of the snowpack.

### 5.2 Spring (April–May)

Spring is a phase of increasing activity in the annual proglacial hydrological cycle. Although mean air temperatures remain low, the onset of continuous daylight in mid-April results in a further gradual increase in the receipt of energy inputs from solar radiation as the sun climbs progressively higher in the sky. While the high albedo of the snowpack continues to offset much of the increase in energy inputs from solar radiation, the potential for snowmelt gradually increases, especially during warmer periods associated with the passage of maritime air masses. Ice layers continue to form beneath and within the proglacial snowpack during such periods. As the sun climbs progressively higher and mean daily air temperatures begin periodically to rise above zero in late May, snowmelt becomes more sustained. However, the onset of runoff is delayed as significant volumes of percolating snowmelt are temporarily stored in the snowpack. The presence of basal ice layers beneath the snowpack prevents percolating snowmelt from accessing the underlying frozen ground surface and may increase lateral flow velocities within the snowpack (Fountain, 1996).

**5.3 Summer (June–September)**

Summer is the most active phase in the annual proglacial hydrological cycle and encompasses the annual melt season (duration about 100 days), during which time mean air temperatures attain an annual maximum and >99% of total annual runoff occurs. During the annual thaw, snowmelt is almost entirely radiation-driven (e.g. Hodgkins, 2001; Hodson et al., 2005), since the controlling influence of the temperature of the snow-covered land surface restricts the sensible heat flux into the snowpack (Nakabayashi *et al*., 1996; Harding & Lloyd, 1997). Melt rates are thus largely similar from year-to-year and the date of the final disappearance of the snowpack and the length of the snow-free period are determined largely by the depth of over-winter snow accumulation at the onset of the melt season (Nakabayashi *et al*., 1996; Harding & Lloyd, 1997).

Runoff usually commences in early June, when the onset of consistently positive mean daily air temperatures triggers rapid and sustained melting of the snowpack. Snowmelt is initially routed laterally within the basal layers of the snowpack to either frozen lake surfaces situated in topographic depressions in the moraine complex or to the surface of the sandur. Increasing inputs of snowmelt from the lower reaches of the main valley glacier initiate the onset of continuous flow in the proglacial channel network by mid-June. By this time, the lake network in the moraine complex is largely thawed and lake levels are high, having been recharged by the receipt of significant volumes of snowmelt. Excess snowmelt is subsequently conveyed as surface runoff in small, ephemeral channels that drain along a topographic gradient from the interior of the moraine complex to the sandur.

The rate of evaporation begins to assume significance following the recession of the snowpack, reflecting the increase in air temperatures and the abundance of surface water available for evaporation. However, as the melt season proceeds, the rate of evaporation gradually declines, reflecting the progressive drying out of the ground surface. Nevertheless, evaporation may exceed precipitation by as much as 235% over the course of the melt season, indicating that water storage in the active layer is sufficient to maintain evaporation during dry periods. Harding & Lloyd (1997) similarly found that total evaporation at elevations <50 m a.s.l. in Svalbard may exceed precipitation by about 160% during the summer.

The first period of significant flow in the proglacial channel network occurs in either late June or early July, in response to sustained melting of the snowpack on the lower reaches of the glacier. By this time, the annual melting of the icing is also usually well under way. However, if prevailing weather conditions are cold and cloudy, the onset of sustained melting of the snowpack and the icing may be delayed until mid-to-late July. Peak flow in the proglacial channel network typically occurs during periods of good weather in mid-to-late July, in response to high rates of ablation on the lower reaches of the glacier. The oversupply of significant volumes of meltwater to the subglacial drainage system during such periods has the potential to trigger subglacial outburst floods, which issue from the glacier terminus and cause the sandur to become flooded for several days (Wadham *et al*., 2001; Cooper, 2003).

Killingtveit et al. (2003) note that runoff is dominated by snowmelt in June and July in Svalbard, while in August and September it is mainly derived from rainfall and glacial melt: catchments with higher proportion of icemelt-supplying glacier cover tend to have relatively higher runoff in August and September than non-glacierized catchments. The return of nights in late August as the sun descends progressively lower in the sky results in a gradual decline in energy inputs from solar radiation throughout the remainder of the summer and a gradual decline in hydrological activity in the proglacial zone. Flow recession occurs in the proglacial channel network, reflecting reduced meltwater inputs from ablation on the glacier, and the rate of evaporation falls sharply, reflecting an increasing excess of outgoing long-wave radiation over incoming short-wave radiation and a progressive cooling of the ground surface prior to the annual freeze-up.

### 5.4 Autumn (October–November)

Autumn is a phase of decreasing activity in the annual proglacial hydrological cycle. The cessation of continuous flow in the proglacial channel network probably occurs in early-to-mid October, when air temperatures begin to fall consistently below zero and the nights become progressively longer. The annual formation of the icing in the area where the western ice-marginal channel issues into the proglacial channel network is initiated by the freezing of subglacial drainage, which continues throughout the autumn months from the artesian upwelling. By the start of November, permanent darkness again prevails and hydrological activity in the proglacial zone essentially becomes dormant, save for inputs of snowfall and the development of the icing.

## 6. Conclusions

Research in high-latitude hydrology remains challenging. Hydrological research infrastructure in high-latitude catchments remains very limited, and the extreme seasonality reduces the utility of many standard techniques, e.g. even where weir structures have been built, they typically fail to capture early-season runoff adequately because of snow- and iceblocking of channels (e.g. Sund, 2008). Significant challenges persist in measuring precipitation reliably and representatively; this not only hinders process analysis and water resources management, but also makes climate change detection difficult (e.g. Førland and Hanssen-Bauer, 2003). Measuring and monitoring the discharge of even moderately-sized, glacially-fed rivers is a demanding task because of the temporal and spatial instability of their flow regimes, particularly if continuous, complete time series are required, as exemplified by the work presented here.

Research into the surface and atmospheric water fluxes of the proglacial zone of Finsterwalderbreen in 1999 has indicated that winter dominates the delivery of precipitation (226 mm $a^{-1}$), while summer is rather dry (29 mm $a^{-1}$). Other parts of Svalbard, such as the north-west, are wetter in summer, to the extent that summer precipitation may occasionally exceed the winter total (Hodson et al., 2005). Measurements and even estimates of evaporation are uncommon in the high latitudes, but a modified version of the general combination model for non-saturated surfaces (Granger & Gray, 1989) worked well in this case, given the availability of a range of meteorological variables, including vapour pressure deficit, wind speed and global radiation, as well as air temperature. Total annual precipitation (255 mm) exceeded total annual evaporation (141 mm) by about 81%, although evaporation can be appreciably in excess of precipitation during the dry summer, indicating short-term water storage, probably in the active layer.

Monitoring of proglacial discharge for 53 days between late-June and mid-August is estimated to have captured 66% of total annual runoff: fluxes outside the monitoring period could be simulated by combining a temperature-index melt model with a runoff regression relationship, an approach which performed well for the instrumental period and was parsimonious in terms of data requirements. 47% of total annual runoff occurred in 23 days encompassing two high-flow periods in early- to mid-summer, so even within the *c*. 100-day melt season, runoff is temporally-concentrated. Despite episodes of flooding, likely leading to short-term water storage, the total annual input and output of runoff to and from the proglacial zone were not significantly different at the timescale of the melt season, indicating that storage is unlikely to have been important overall, or from season to season.

A range of uncertainties are associated with the fluxes derived by measurement, modelling and estimation in this paper, but these can be rigorously quantified probabilistically. The greatest flux uncertainties are associated with runoff, because it is at least an order-of-magnitude higher than any other flux, e.g. total glacial runoff delivered to the sandur is $7.38\times10^7$ $m^3$ $a^{-1}$, whereas the total precipitation flux to the sandur is $2.29\times10^5$ $m^3$ $a^{-1}$. However, the proportional uncertainty associated with precipitation is two-and-a-half times that associated with runoff, mainly as a result of the considerable spatial heterogeneity in winter accumulation.

The synthesised description of the seasonal hydrological cycle presented above can be viewed as a set of hydrological boundary conditions, serving as a context for understanding fluvial material fluxes from this and similar catchments, and as a basis for assessing the effects of climate change on local and regional hydrological regimes. A companion paper to this one will look at the sub-surface fluxes in the Finsterwalderbreen catchment, and at the complete annual water budget.

**Acknowledgments**

This work was funded by the NERC ARCICE Thematic Programme grant GST/02/2204 and tied studentship GT24/98/ARCI/8. We would like to thank the Norsk Polarinstitutt for logistical support and Deborah Jenkins, Elizabeth Farmer, Andrew Terry and Catherine Styles for assistance in the field.

## References

Anisimov, O.A., Vaughan, D.G., Callaghan, T.V., Furgal, C., Marchant, H., Prowse, T.D., Vilhjálmsson, H., Walsh, J.E., 2007. Polar regions (Arctic and Antarctic). Climate Change 2007: Impacts, Adaptation and Vulnerability. Contribution of Working Group II to the Fourth Assessment Report of the Intergovernmental Panel on Climate Change. M.L. Parry, O.F. Canziani, J.P. Palutikof, P.J. van der Linden and C.E. Hanson (Eds.), Cambridge University Press, Cambridge, 653–685.

Bates, B.C., Kundzewicz, Z.W., Wu, S., Palutikof, J.P., Eds., 2008. Climate Change and Water. Technical Paper of the Intergovernmental Panel on Climate Change, IPCC Secretariat, Geneva, 210 pp.

Bruce, J.P., Clark, R.H., 1990. Introduction to Hydrometeorology (2nd Edition). Pergamon, Toronto.

Cooper, R.J. 2003. Chemical denudation in the proglacial zone of Finsterwalderbreen, Svalbard. Unpublished Ph.D. thesis, University of Bristol.

Cooper, R.J., Wadham, J.L., Tranter, M., Hodgkins, R., Peters, N., 2002. Groundwater hydrochemistry in the active layer of the proglacial zone, Finsterwalderbreen, Svalbard. Journal of Hydrology, 269, 208–223.

Dallmann, W.K., Hjelle, A., Ohta, Y., Salvigsen, O., Bjornerud, M.G., Hauser, E.C., Maher, H.D., Craddock, C., 1990. Geological map of Svalbard 1:100 000: Sheet B11G Van Keulenfjorden. Norsk Polarinstitutt, Oslo.

Førland, E.J., Hanssen-Bauer, I. 2003. Past and future climate variations in the Norwegian Arctic: overview and novel analyses. Polar Research 22(2), 113–124.

Fountain, A.G., 1996. Effect of snow and firn hydrology on the physical and chemical characteristics of glacial runoff. Hydrological Processes, 10, 509–521.

French, H.M., 2007. The Periglacial Environment (3rd Edition). Wiley, Chichester.

Fox, A.J., 1995. Finsterwalderbreen. British Antarctic Survey, Cambridge.

Granger, R.J., Gray, D.M., 1989. Evaporation from natural nonsaturated surfaces. Journal of Hydrology, 111, 21–29.

Hagen, J.O., Etzelmüller, B., Nuttall, A.-M., 2000. Runoff and drainage pattern derived from Digital Elevation Models, Finsterwalderbreen, Svalbard. Annals of Glaciology, 31, 147–152.

Hanssen-Bauer, I., Kristensen Solås, M., Steffensen, E.L., 1990. The climate of Spitsbergen. Norsk Meteorologiske Institutt Rapport, 39/90.

Harding, R.J., Lloyd, C.R., 1997. Fluxes of water and energy from three high latitude tundra sites in Svalbard. Nordic Hydrology, 29, 267–284.

Hock, R., 2003. Temperature index melt modelling in mountain areas. Journal of Hydrology, 282, 104–115.

Hodgkins, R., 1997. Glacier hydrology in Svalbard, Norwegian High Arctic. Quaternary Science Reviews, 16, 957–973.

Hodgkins, R., Tranter, M., Dowdeswell, J.A. 1997. Solute provenance, transport and denudation in a High-Arctic glacierised catchment. Hydrological Processes, 11(4), 1813–1832.

Hodgkins, R., 2001. Seasonal evolution of meltwater generation, storage and discharge at a non-temperate glacier in Svalbard. Hydrological Processes, 15(3), 441–460.

Hodgkins, R., Cooper, R., Wadham, J., Tranter, M., 2003. Suspended sediment fluxes in a High-Arctic glacierised catchment: implications for fluvial sediment storage. Sedimentary Geology, 165, 105–117.

Hodgkins, R., Tranter, M., Dowdeswell, J.A., 2004. The characteristics and formation of a High-Arctic proglacial icing. Geografiska Annaler, 86A(3), 265–275.

Hodgkins, R., Cooper, R., Wadham, J., Tranter, M., 2005. Inter-annual variability in the spatial distribution of winter accumulation at a High-Arctic glacier (Finsterwalderbreen, Svalbard), and its relationship with topography. Annals of Glaciology, 42, 243–248.

Hodgkins, R., Fox, A.J., Nuttall, A.-M., 2007. Geometry change between 1990 and 2003 at Finsterwalderbreen, a Svalbard surge-type glacier, from GPS profiling. Annals of Glaciology, 46, 131–135.

Hodson, A.J., Ferguson, R.I., 1999. Fluvial suspended sediment transport from cold and warm-based glaciers in Svalbard. Earth Surface Processes and Landforms, 24(11), 957–974.

Hodson, A., Gurnell, A., Washington, R., Tranter, M., Clark, M., Hagen, J.O., 1998. Meteorological and runoff time-series characteristics in a small, high-Arctic glaciated basin, Svalbard. Hydrological Processes, 12, 509–526.

Hodson, A., Kohler, J., Brinkhaus, M., 2005. Multi-year water and surface energy budget of a high-latitude polythermal glacier: evidence for overwinter water storage in a dynamic subglacial reservoir. Annals of Glaciology 42, 42–46.

Killingtveit, A., Pettersson, L.-E., Sand, K. 2003. Water balance investigations in Svalbard. Polar Research, 22(2), 161–174.

Krigstom, A., 1962. Geomorphological studies of sandur plains and their braided rivers in Iceland. Geografiska Annaler, 44, 328–346.

Nakabayashi, H., Kodama, Y., Takeuchi, Y., Ozeki, T., Ishikawa, N., 1996. Characteristics of heat balance during snowmelt season in Ny-Ålesund, Spitsbergen island. In Watanabe, O. (Ed.), Memoirs of National Institute of Polar Research, Tokyo, Special Issue no. 51, 255–266.

Nuttal, A.M., Hodgkins, R. 2005. Long-term dynamics and mass balance of Finsterwalderbreen, a Svalbard surge-type glacier. Annals of Glaciology, 42, 71–76.

Nuttall, A-M., Hagen, J.O., Dowdeswell, J.A. 1997. Quiescent-phase changes in velocity and geometry of Finsterwalderbreen, a surge-type glacier in Svalbard. Annals of Glaciology, 24, 249–254.

Repp, K., 1988. The hydrology of Bayelva, Spitsbergen. Nordic Hydrology, 19, 259–268.

Sund, M., 2008. Polar hydrology – Norwegian Water Resources and Energy Directorate's work in Svalbard. Norwegian Water Resources and Energy Directorate Report 2-2008.

Synergy Software, 1997. KaleidaGraph (4th Edition). Synergy Software, Reading, Pennsylvania.

Topping, J., 1972. Errors of Observation and their Treatment (4th Edition). Chapman and Hall, London.

Vatne, G., Etzelmüller, B., Sollid, J.L., Ødegård, R.S., 1995. Hydrology of a polythermal glacier, Erikbreen, northern Spitsbergen. Nordic Hydrology, 26(3), 169–190.

Vatne, G., Etzelmüller, B., Ødegård, R.S., Sollid, J.L., 1996. Meltwater routing in a high arctic glacier, Hannabreen, northern Spitsbergen. Norsk Geografisk Tidsskrift, 50, 67–74.

Wadham, J.L., Hodson, A.J., Tranter, M., Dowdeswell, J.A., 1997. The rate of chemical weathering beneath a quiescent, surge-type, polythermal-based glacier, southern Spitsbergen, Svalbard. Annals of Glaciology, 24, 27–31.

Wadham, J.L., Hodson, A.J., Tranter, M., Dowdeswell, J.A., 1998. The hydrochemistry of meltwaters draining a polythermal-based, high Arctic glacier, south Svalbard: I. The ablation season. Hydrological Processes, 12, 1825–1849.

Wadham, J.L., Tranter, M., Dowdeswell, J.A., 2000. Hydrochemistry of meltwaters draining a polythermal-based, high-Arctic glacier, south Svalbard: II. Winter and early Spring. Hydrological Processes, 14, 1767–1786.

Wadham, J.L., Cooper, R.J., Tranter, M., Hodgkins, R., 2001. Enhancement of glacial solute fluxes in the proglacial zone of a polythermal glacier. Journal of Glaciology, 47 (158), 378–386.

Willis, I.C., 2005. Hydrology of Glacierized Basins. In Anderson, M.G. (Ed.), Encyclopaedia of Hydrological Sciences. Chichester, Wiley.

Ødegård, R.S., Hagen, J.O., Hamran, S., 1997. Comparison of radio echosounding (30 MHz–

1000 MHz) and high resolution borehole temperature measurements at Finsterwalderbreen, southern Spitsbergen, Svalbard. Annals of Glaciology, 24, 262–267.

## Figure captions

Fig. 1. (Clockwise from top left) Location of Finsterwalderbreen within the Svalbard archipelago (inset). Topographic map of the glacier terminus and proglacial area, elevations in m a.s.l. (Fox, 1995). 1995 aerial photograph of the glacier terminus and proglacial area (subset of aerial photograph S95 1113© Norwegian Polar Institute): discharge monitoring locations are indicated (note that many stream courses apparent on the map and photograph, e.g. X, are not currently active, and that all of the runoff from the catchment is channelled through the outlet); the locations of the Automatic Weather Station (AWS) and a Wells Transect (WT), used to monitor sub-surface water fluxes, are also indicated. Upstream views of the Outlet on 24 June (discharge ca. 5 $m^3 s^{-1}$) and 21 July (discharge ca. 25 $m^3 s^{-1}$) 1999; the lighter colour of the runoff on 21 July is a result of the angle of the sun, rather than lower turbidity. High-elevation view of the Finsterwalderbreen proglacial area looking northeast, showing discharge monitoring locations (although the East gauge is just off the right of the image).

Figure 2. Meteorological time-series from the AWS located in the proglacial zone. (A) Air temperature (˚ C). (B) Vapour pressure deficit (kPa). (C) Wind Speed (m $s^{-1}$). (D) Global radiation (W $m^{-2}$). (E). Precipitation as rainfall (mm). Days of year 110–330 correspond to 20 April–26 November.

Figure 3. Time series of daily (A) radiation flux (MJ $m^{-2}$; NSWR, NLWR and NAWR are Net Short-Wave, Net Long-Wave and Net All-Wave Radiation Fluxes, respectively) and (B) evaporation from the surface of the proglacial zone (mm). Days of year 110–330 correspond to 20 April–26 November.

Figure 4. Time series of (A) stage (m) and (B) discharge ($m^3$ $s^{-1}$) at each of the gauges. Terminus West and East constitute inputs to the proglacial channel network, and Outlet constitutes output. Days of year 175–230 correspond to 24 June–18 August.

Figure 5. Time series of daily (A) measured and modelled glacier ablation (mm w.e.) and (B) measured and estimated (from the regression of Outlet discharge on modelled melt) total surface water flux from the proglacial zone ($m^3$). Days of year 110–330 correspond to 20 April–26 November.

**Tables**

| Gauge | Compilation Period | Equation | *n* | $R^2$ | *s.e.* (%) |
|---|---|---|---|---|---|
| Outlet | 17:00 175–12:00 229 | $Q_O = 1.43e^{3.23S}$ | 13 | 0.99 | 4.4 |
| Terminus West | 17:00 183–12:00 187 | $Q_W = 19.5S + 1.28$ | 2 | - | - |
| Terminus West | 16:00 191–12:00 195 | $Q_W = 5.76S + 2.57$ | 2 | - | - |
| Terminus West (interpolation)[a] | 17:00 175–16:00 183<br>13:00 187–15:00 191<br>13:00 195–10:00 229 | $Q_W = Q_O - Q_E$ | - | - | - |
| Terminus East | 16:00 183–15:00 195 | $Q_E = 16.4S + 1.16$ | 9 | 0.98 | 12.5 |
| Terminus East (interpolation)[a] | 17:00 175–15:00 183;<br>16:00 195–10:00 229 | $Q_E = 0.30Q_O + 0.67$ | - | 0.71 | 9.4 |

Table 1. Summary of rating curves compiled at each gauge during the 1999 discharge monitoring period, together with interpolations used when adequate ratings could not be determined. $Q$ is discharge (m$^3$ s$^{-1}$) and subscripts $O$, $W$ and $E$ denote discharge at the Outlet, Terminus West and Terminus East gauges, respectively. $S$ is stage (m), $n$ is the number of discharge measurements, $R^2$ is the coefficient of determination and *s.e.* is the standard error of the regression. [a]$Q_O$ has been lagged by 1 hour to account for the mean transit time between the glacier terminus and the Outlet.

| Period | $E_T$ | $E_{WS}$ | $E_{VPD}$ | $E_G$ | $E_{AV}$ | $E_{EM}$ | $E_P$ |
|---|---|---|---|---|---|---|---|
| 13:00 113 1999–20:00 85 2000 | 2.0$^{(3)}$ | 10.0 | 2.0 | 2.5 | 10.0$^{(6)}$ | 7.2 | 27.8 |

Table 2. Summary of probable errors in the calculation of evaporation water flux from the proglacial zone. Potential errors (±%) are associated with the measurement of air temperature ($E_T$), wind speed ($E_{WS}$), vapour pressure deficit ($E_{VPD}$) and global radiation ($E_G$); other potential errors are associated with the use of assumed values ($E_{AV}$) and the standard error from empirical models ($E_{EM}$). $E_P$ is the probable error range of calculated evaporation values for the specified time period. Figures in brackets denote the number of times each potential source of error arose during calculations.

| **Gauge** | **Period** | $E_S$ | $E_V$ | $E_D$ | $E_{RC}$ | $E_{RM}$ | $E_P$ |
|---|---|---|---|---|---|---|---|
| Outlet | 17:00 175–10:00 229 | 0.1 | 2.2 | 10.0 | 4.4 | - | 11.1 |
| Terminus West | 17:00 175–16:00 183 | - | - | - | - | - | 18.4[a] |
| Terminus West | 17:00 183–12:00 187 | 0.1 | 2.2 | 10.0 | 10.0[b] | - | 14.3 |
| Terminus West | 13:00 187–15:00 191 | - | - | - | - | - | 16.4[a] |
| Terminus West | 16:00 191–12:00 195 | 0.1 | 2.2 | 10.0 | 10.0[b] | - | 14.3 |
| Terminus West | 13:00 195–10:00 229 | - | - | - | - | - | 18.4[a] |
| Terminus East | 17:00 175–15:00 183 | - | - | - | - | 9.4 | 14.6[c] |
| Terminus East | 16:00 183–15:00 195 | 0.1 | 2.2 | 10.0 | 6.4 | - | 12.1 |
| Terminus East | 16:00 195–10:00 229 | - | - | - | - | 9.4 | 14.6[3] |

Table 3. Summary of probable errors in the time series of discharge at each gauge during the 1999 monitoring period. Potential errors (±%) are associated with the measurement of stage ($E_S$), the measurement of flow velocity ($E_V$), the measurement of channel depth ($E_D$), the relevant rating curve ($E_{RC}$), the regression used for interpolation (Table 1)($E_{RM}$); $E_P$ is the probable error range of discharge data for the specified time period. [a]indicates value determined by probabilistically combining  relevant values of $E_P$ at the Outlet and Terminus East, [b]indicates value is a maximum estimate and [c]indicates value determined by probabilitistically combining value of $E_{RM}$ with relevant value of $E_P$ at the Outlet.

Figure 1
Click here to download high resolution image

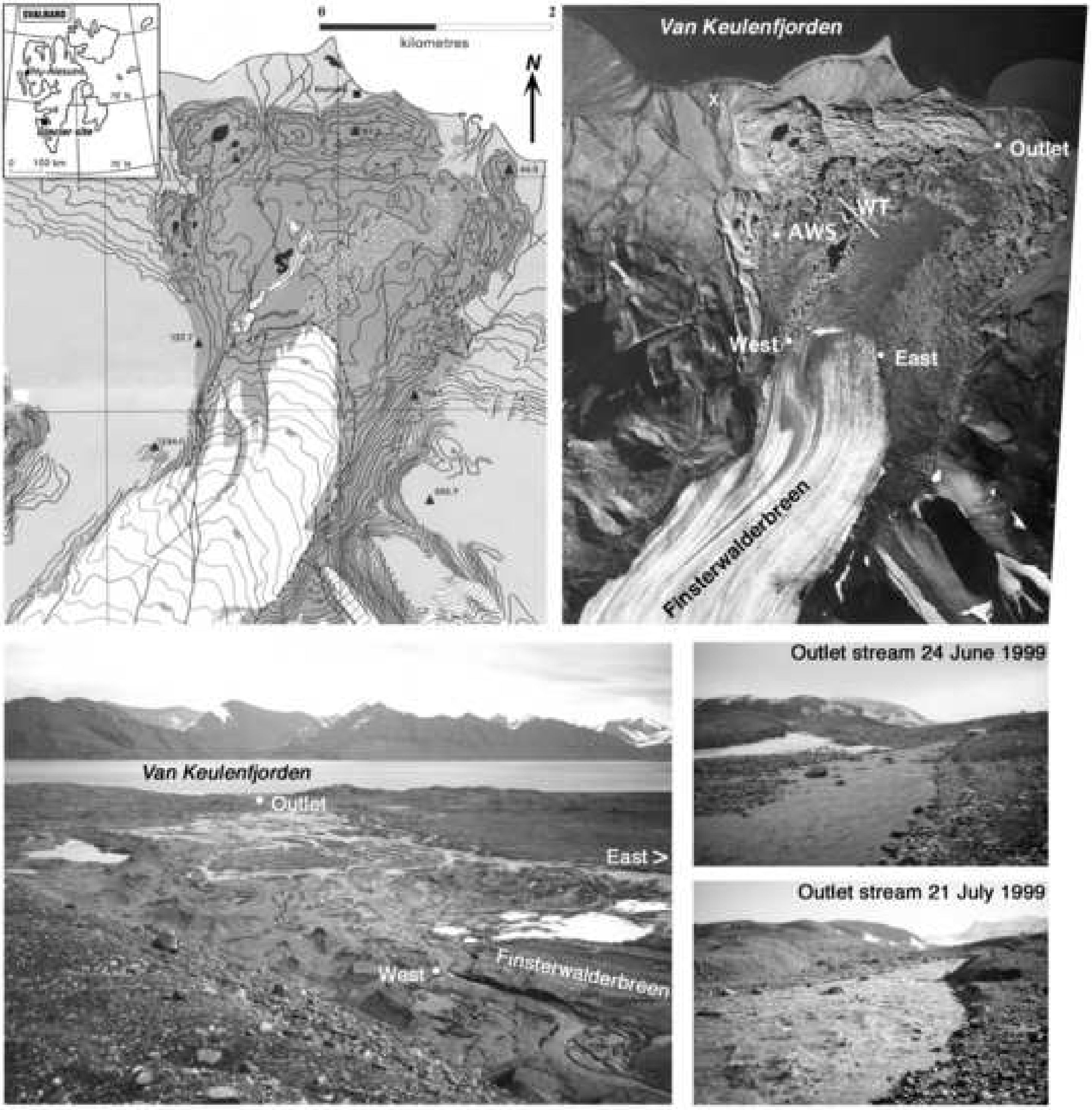

Figure 2

Click here to download high resolution image

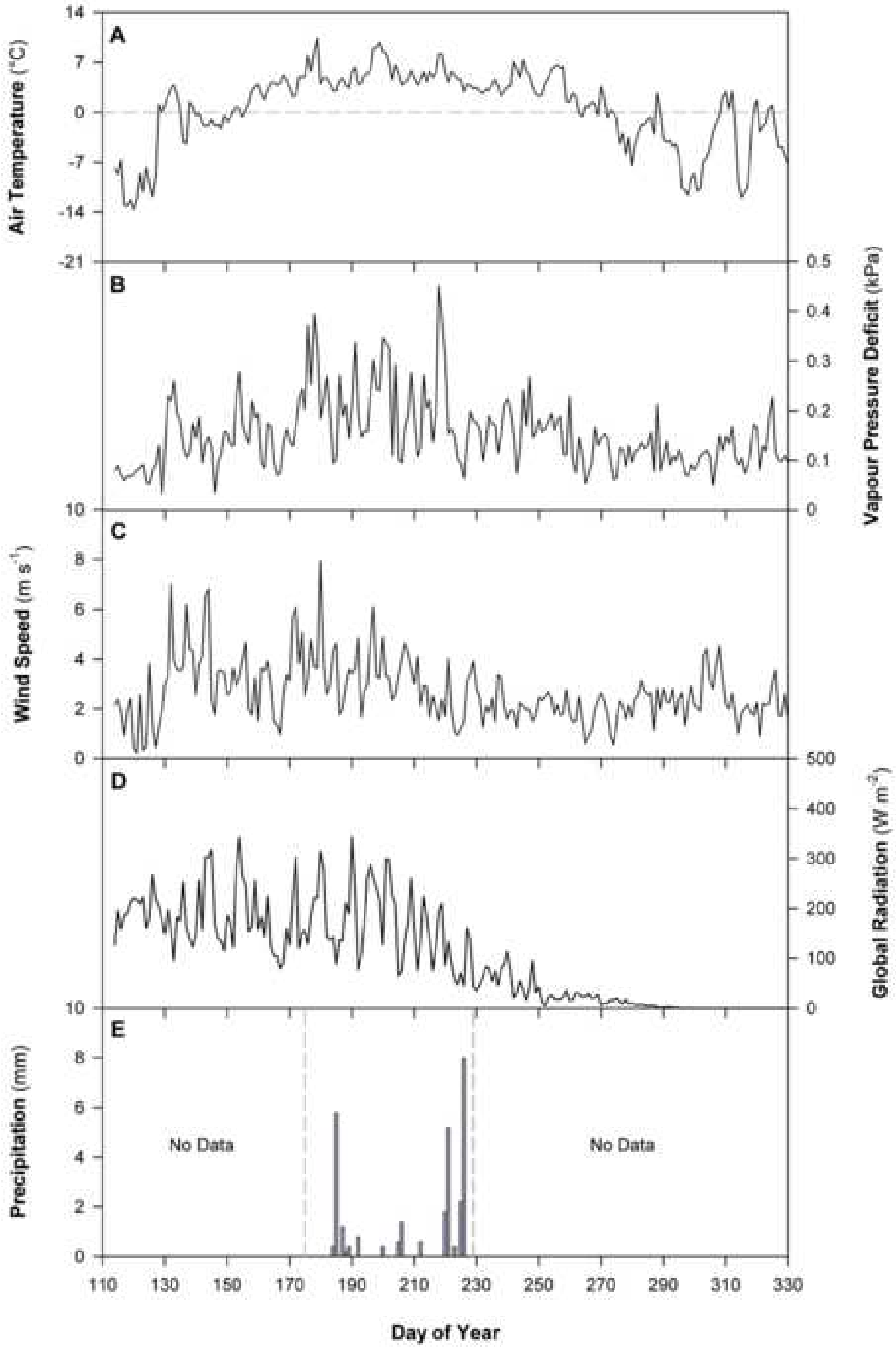

Figure 3
Click here to download high resolution image

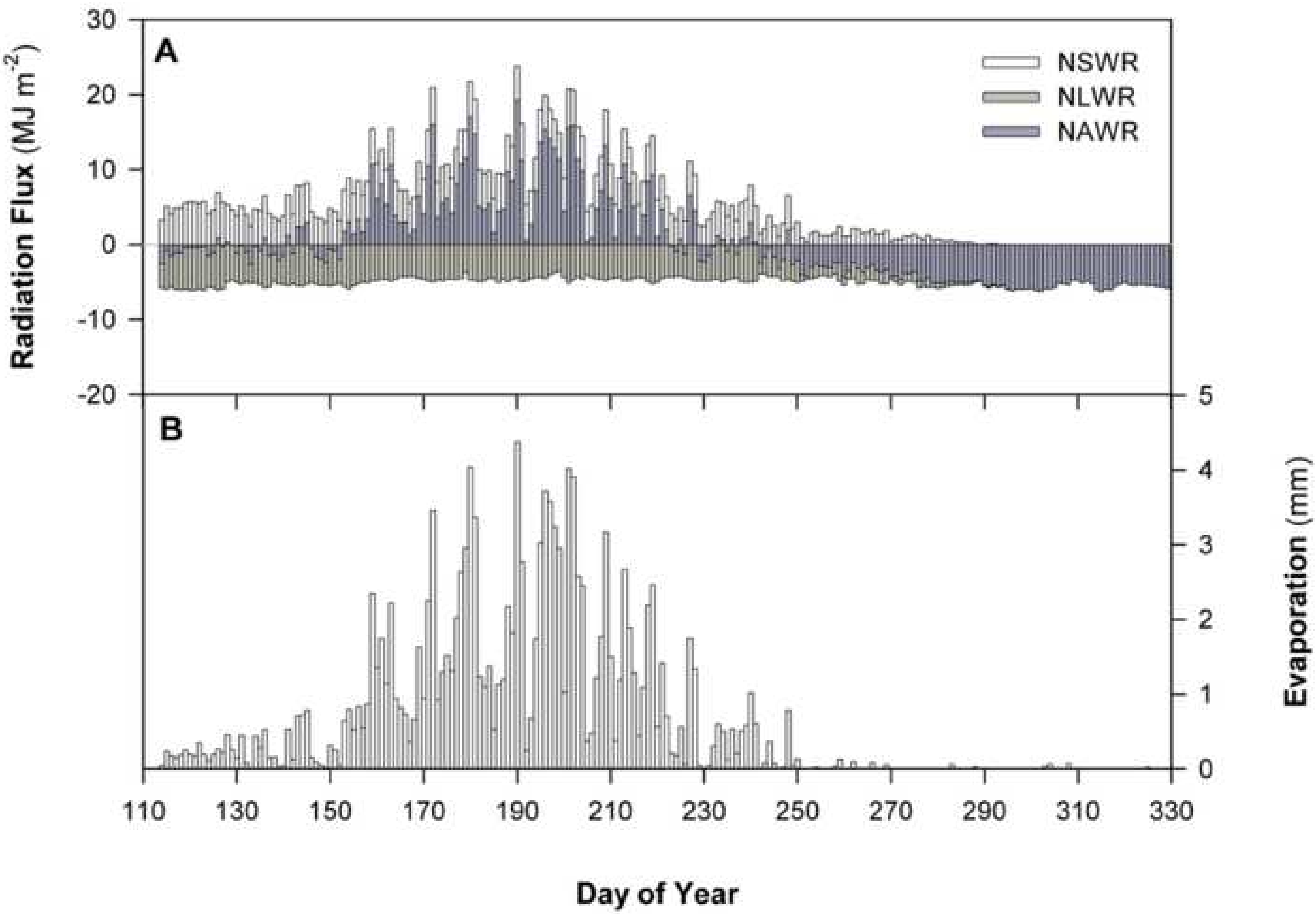

Figure 4

Click here to download high resolution image

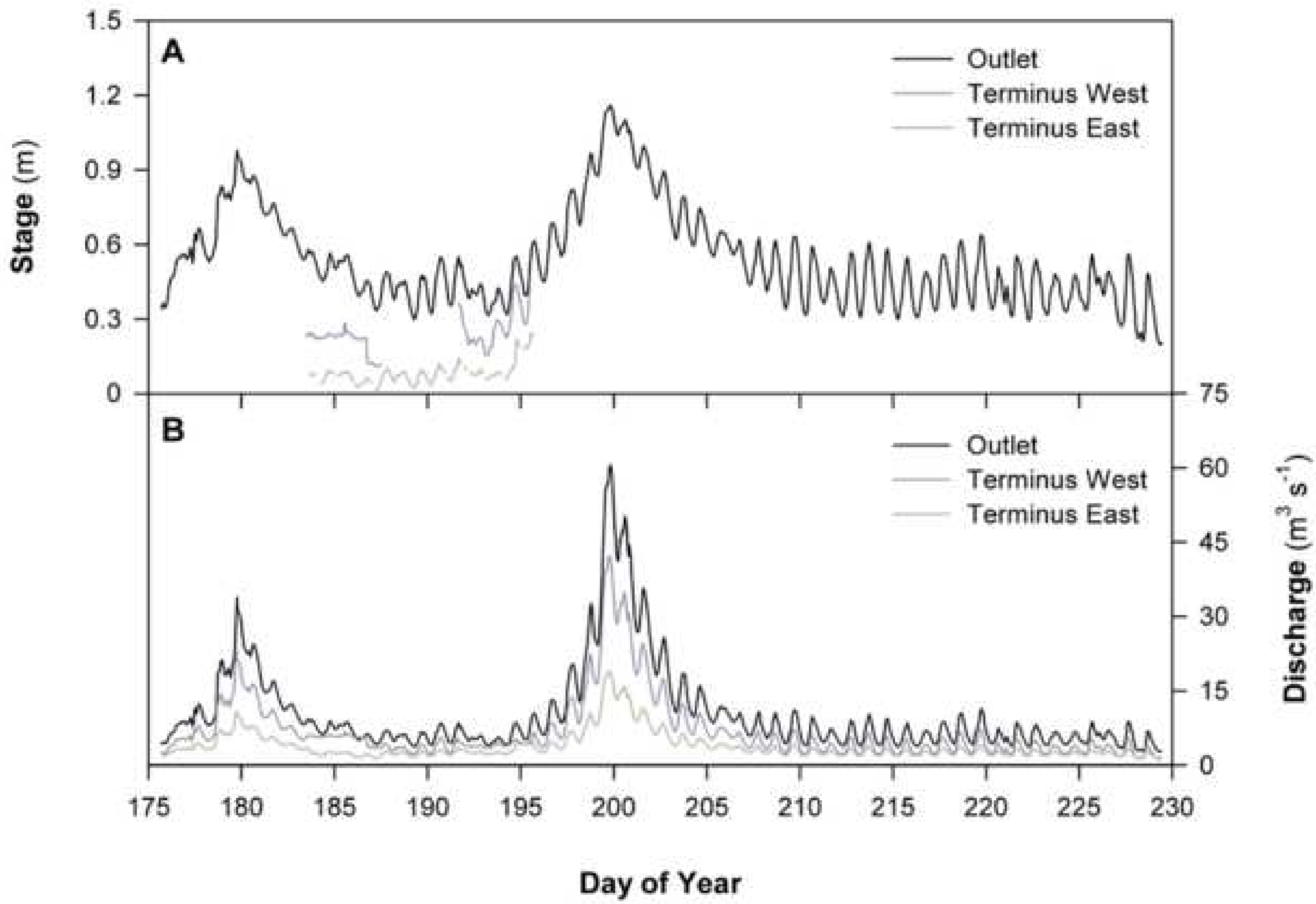

Figure 5

Click here to download high resolution image